Analytical and Numerical Prediction of Concentration Profiles in Microfluidic Gradient Generators

Rob Chambers

March 23, 2007

1 Introduction

A host of recent microfluidic devices have been developed to create known and temporally stable chemical gradients. In one common design, a cascade of diffusive mixers recombine in a wide, shallow channel to yield an approximately linear concentration gradient.[1] The resulting concentration gradient can be used to study cell cell processes such as chemotaxis, differentiation, and proliferation. The concentration profile in these devices is often assumed to remain linear and constant throughout the length of the chamber, even though diffusion does cause the profile to decay. To combat this, high flow rates can be used to minimize the residence time of the fluid. However, high flow rates are known to impact the direction of cell migration. Consequently, a simple model of diffusion processes would be helpful in device design and evaluation. Presented below is an analytical model which employs Taylor-Aris dispersion to simplify the problem to 2-D steady-state diffusion. This problem is then solved using a separation of variables approach. Finally, the model's predictions are compared with those of full 3-D numerical simulation.

2 Theory

2.1 Taylor-Aris Dispersion

Laminar fluid flow in a wide, shallow rectangular channel can be approximated, far from the side walls, as plane Poiseuille flow with velocity given by:

$$u(y) = U_o + u'(y) = U_o + \frac{3}{2}U_o\left(\frac{1}{3} - \left(\frac{2y}{h}\right)^2\right) \tag{1}$$

where U_o is the bulk velocity and h is the channel height. The area-averaging approach described in the ME457 notes can be used to determine the Taylor-Aris dispersion coefficient, D_{eff}. The mathematics are similar, as are the scalings, except that the smallness parameters

become $\epsilon \sim \frac{h}{L} \sim \frac{U_o h^2}{DL} \ll 1$, where D is the intrinsic diffusivity of the solute and L is the position of interest. Furthermore, the final integration becomes:

$$\left\langle u' \frac{\partial C'}{\partial x} \right\rangle = \frac{1}{h} \int_{-h/2}^{h/2} \frac{3}{2} U_o \left(\frac{1}{3} - \left(\frac{2y}{h} \right)^2 \right) \frac{U_o h^2}{2D} \frac{\partial^2 \langle C \rangle}{\partial x^2} \left(\frac{y^2}{2h^2} - \frac{y^4}{h^4} \right) dy \tag{2}$$

$$= -\frac{U_o^2 h^2}{210D} \frac{\partial^2 \langle C \rangle}{\partial x^2} \tag{3}$$

Continuing with the approach used in the notes, the effective dispersion coefficient becomes:

$$D_{\text{eff}} = D + \frac{U_o^2 h^2}{210D} \tag{4}$$

(Note: calculation using the channel half-height would result in a coefficient of $2/105$ instead of $1/210$.) It will be helpful to our subsequent discussion to define a diffusivity ratio γ:

$$\gamma = \frac{D_{\text{eff}}}{D} = 1 + \frac{U_o^2 h^2}{210 D^2} \tag{5}$$

Thus, for slow flows in shallow channels, γ can approach its minimum value of 1. However, there is no maximum γ as long as we remain in the Taylor-Aris regime, and the Taylor-Aris regime can always be obtained if the region of interest is sufficiently far downstream.

2.2 Solution of the Convective Diffusion Equation

Consider a long, thin channel of width $2w$, height $h \ll 2w$, and bulk-averaged fluid velocity U_o. Ignoring the attenuated flow near the channel edges, and applying the results of the Taylor-Aris dispersion analysis, we can model the system as uniform plug flow with velocity U_o, diffusivity D_{eff} in the streamwise direction $\hat{x}$, and diffusivity D in the spanwise direction $\hat{y}$. Under these assumptions, the concentration c of a dilute solute is governed by the 2-D convective diffusion equation:

$$U_o \frac{\partial c}{\partial x} = D_{\text{eff}} \frac{\partial^2 c}{\partial x^2} + D \frac{\partial^2 c}{\partial y^2} \tag{6}$$

Defining the nondimensional variables $\xi = x/w$, $\eta = y/w$, and $\Theta = (c - c_{\text{avg}})/c_o$, the convective diffusion equation becomes:

$$\text{Pe}_w \frac{\partial \Theta}{\partial \xi} = \gamma \frac{\partial^2 \Theta}{\partial \xi^2} + \frac{\partial^2 \Theta}{\partial \eta^2} \tag{7}$$

where $\gamma = D_{\text{eff}}/D$ (as in Eq. 5) and $\text{Pe}_w = U_o w/D$, with boundary conditions:

$$\Theta(\xi = 0, \eta) = f(\eta) \tag{8}$$

$$\Theta_\xi(\xi = \infty, \eta) = 0 \tag{9}$$

$$\Theta_\eta(\xi, \eta = \pm 1) = 0 \tag{10}$$

Separating $\Theta = F(\xi)G(\eta)$:

$$\frac{G''}{G} = \frac{-\gamma F'' + \mathrm{Pe}_w F'}{F} = -\lambda^2 \tag{11}$$

Using the boundary conditions of Eq. 10, G becomes a Fourier series:

$$G_n = a_n \sin\frac{n\pi}{2}\eta + b_n \cos(\frac{n\pi}{2}), n = 0, 1, 2, ... \tag{12}$$

with the restriction that a_n=0 for n even, and b_n=0 for n odd. This sine-cosine series is attenuated for increasing ξ by the decaying exponential:

$$F_n = \exp\left\{-\frac{\mathrm{Pe}_w}{2\gamma}\left(\sqrt{1+\gamma\left(\frac{n\pi}{\mathrm{Pe}_w}\right)^2} - 1\right)\xi\right\} \tag{13}$$

For small wavenumbers and large Pe_w, this equation reduces to that obtained if streamwise diffusion is neglected (i.e., $\gamma = 0$):

$$F_n = \exp\left\{\frac{(n\pi)^2}{2\mathrm{Pe}_w}\xi\right\} \tag{14}$$

For high wave numbers, large γ, and small Pe_w, the actual value of Pe_w becomes irrelevant:

$$F_n = \exp\left\{\frac{n\pi}{2\sqrt{\gamma}}\xi\right\} \tag{15}$$

Thus, the behavior of the concentration profile at low ξ is dominated by the attenuation of high-spatial-frequency components by spanwise diffusion. At large ξ these components vanish and the attenuating spanwise diffusion is partially counteracted by streamwise diffusion, which serves to maintain the profile further downstream.

In many practical applications, the region of interest is sufficiently far downstream that low-wave-number components are dominant. It is instructive to consider when, if ever, streamwise diffusion (as measured by γ) significantly affects this region. By setting the second term inside the radical in Eq. 13 equal to one, and my considering the lowest wavenumber ($n = 1$), we can estimate the crossover point γ_c at which γ begins to dominate the system's far-field behavior:

$$\gamma_c = \left(\frac{\mathrm{Pe}_w}{n\pi}\right)^2 \approx .1 \cdot \mathrm{Pe}_w^2 \tag{16}$$

2.3 Fourier Series Approximation of Practical Concentration Profiles

The Fourier series formulation detailed above can represent any practical inlet concentration profile, and recent work has demonstrated nonlinear and even arbitrary profiles.[2] However, three inlet concentration profiles are of particular relevance to recent microfluidic gradient

generators. With the concentration nondimensionalized as above, with $\Theta = (c - c_{\text{avg}})/c_o$, all three of these profiles are odd functions with no DC offset (i.e., $\Theta(\eta) = \Theta(-\eta)$), so that $b_n = 0$ and the Fourier series reduces to a Fourier sine series.

The first profile of interest is a single *step profile* in which two initially uniform streams flow in parallel. This profile is represented by the Fourier coefficients:

$$a_n = \frac{4}{n\pi} \qquad n = 1, 3, 5, \ldots \tag{17}$$

The second profile of interest is the *staircase profile* which consists of k concentration steps. The step profile given above is simply a staircase profile with $k = 2$. For k odd, the Fourier coefficients of the staircase profile are given by:

$$a_n = \frac{8}{k-1} \sum_{j=1}^{\frac{k-1}{2}} \frac{\sin(n\pi j/k) \sin(n\pi/2)}{n\pi} \qquad n = 1, 3, 5, \ldots \tag{18}$$

The third profile of interest is the *linear profile*, which is an idealized staircase profile in which $k \to \infty$. While no inlet profile is truly linear, this idealization is often used with some success to predict downstream concentration gradients for devices with high k. Furthermore, the decay of its low-frequency components can be used to predict the far-field decay time of all three of these initial profiles. Its coefficients are given by:

$$a_n = \frac{8(-1)^{(n-1)/2}}{n^2\pi^2} \qquad n = 1, 3, 5, \ldots \tag{19}$$

3 3-D Numerical Simulation

A model of the 3-D convective diffusion problem was implemented in COMSOL Multiphysics. The diffusion chamber was represented as a rectangular prism. Following the nondimensionalization used above, the chamber had a width in the $\hat{y}$ direction of 2, a height in the $\hat{z}$ direction of $\alpha = h/w$, and a length in the $\hat{x}$ direction of L/w.

Diffusion was implemented with the convective diffusion function of COMSOL's MEMS Module. The isotropic diffusivity was arbitrarily set to $D = 1$. Fluid velocity was modeled as above, with

$$u(z) = \text{Pe}_w \frac{3}{2} \left(1 - \left(\frac{2y}{\alpha} \right)^2 \right) \tag{20}$$

Consequently, the physics of the model were prescribed by entirely by the Peclet number Pe_w and the aspect ratio α. Adaptive mesh refinement was used to bring the number of mesh elements to roughly 30,000.

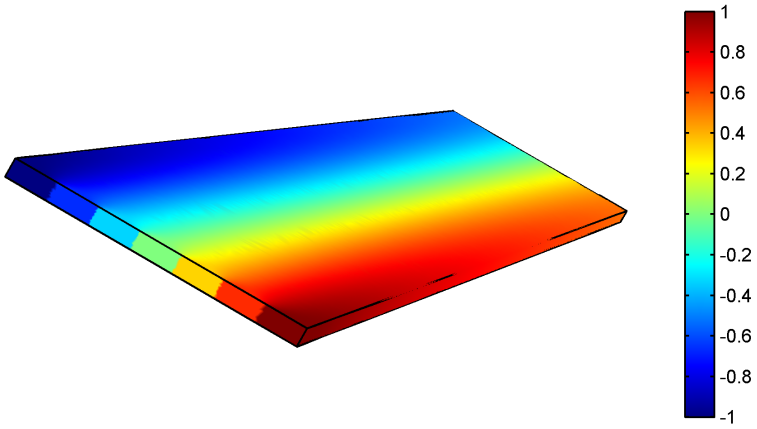

Figure 1: Boundary plot of a 3-D simulation of case B. The inlet concnetration profile consists of seven "'steps"' of equal width. This profile is quickly smoothed by diffusion, and becomes a decaying half-cosine downstream. These profiles are shown more quantitatively in Fig. 4.

4 Results

Simulation results for two cases are presented below. The first, *Case A*, uses the same parameters and an initial concentration profile as Lin et al..[1] The second, *Case B*, modifies those parameters slightly to bring the problem further into the Taylor Dispersion regime.

	$2 \cdot w$ [μm]	U_o [μm/s]	h [μm]	L [cm]
Case A	175	380	100	1.2
Case B	400	100	50	1.2

Table 1: Dimensional Parameters

	Pe_w	γ	$\frac{U_o h^2}{DL}$	$\frac{\gamma}{.1 \cdot \mathrm{Pe}_w^2}$
Case A	222	77	1.1	.016
Case B	133000	2.3	.070	$1.3 \cdot 10^{-9}$

Table 2: Nondimensional Parameters

Note that Case A does *not* fulfill the condition that $\frac{U_o h^2}{DL} \ll 1$; consequently, transverse concentration gradients may be significant.

Both cases used a 7-step staircase profile at the fluid inlet. Results results of the numerical simulation of case B are shown in Fig. 1, and more detailed analysis follows below.

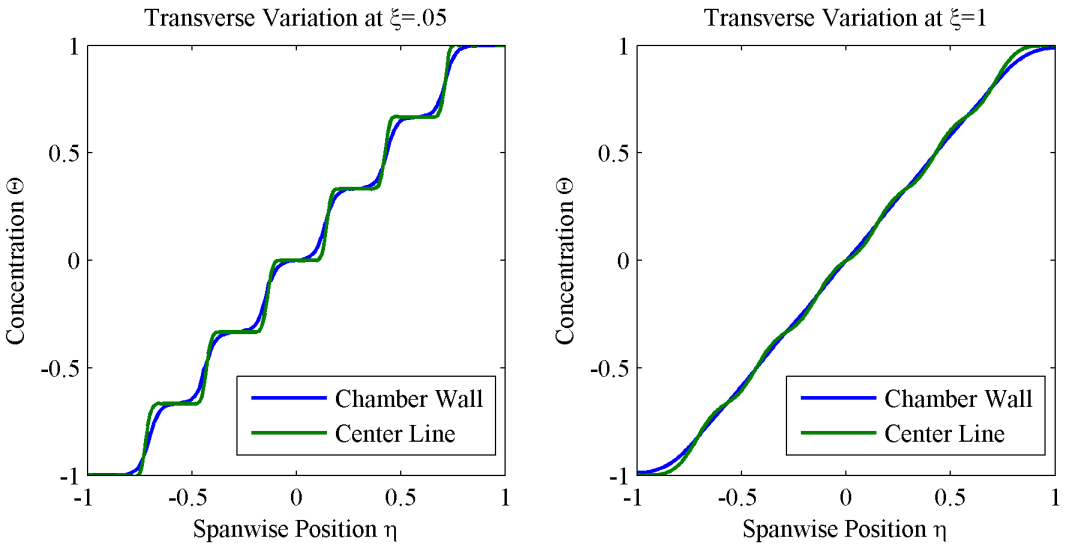

Figure 2: Concentration profiles for case A at $\xi = .05$ and $\xi = 1$, for both the center of the chamber and the chamber wall. The significant differences between the two profiles close to the inlet (left) are substantially smoothed downstream (right).

4.1 Transverse Concentration Gradients

While the analytical model developed in previous sections predicts a 2-D depth-averaged concentration, most applications of microfluidic gradient generators require knowledge of the 3-D field. For instance, experiments involving adherent cells depend on concentrations near the chamber wall, which can differ from those along the centerline. Furthermore, even transverse gradients may affect cell behavior.

Plotted in Fig. 2 are concentration profiles in Case A at the chamber wall and at the centerline for $\xi = .05$ and $\xi = 1$. These positions corresponding to downstream distances of 8.75μm and 175μm, and smallness parameters $\frac{U_o h^2}{DL}$ of 1500 and 75, respectively. Encouragingly, the transverse variation essentially vanishes by $\xi = 1$, even though the smallness parameter is clearly much greater than 1. In the region of interest at $L = 1.2$cm, variations are virtually nonexistant.

4.2 Downstream Concentration Profiles

Figures 3 and 4 show predicted downstream concentration profiles for cases A and B. Due to the length of the chamber in these simulations, computer memory constraints limited the accuracy of the numerical solution for small ξ in case A. However, both cases show excellent agreement between analytical and numerical predictions.

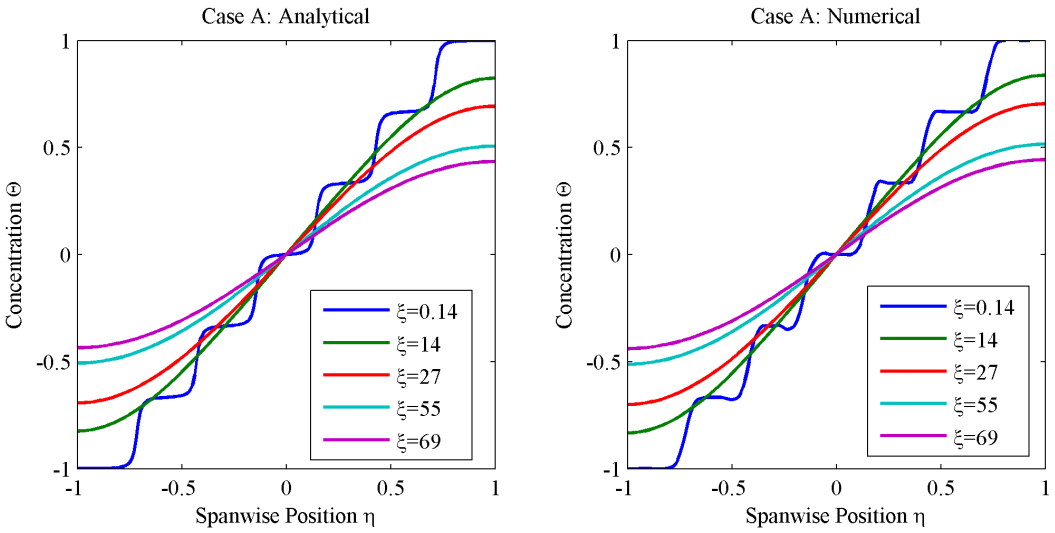

Figure 3: Concentration profiles for case A at several streamwise positions. The analytical and numerical predictions show excellent agreement. The numerical results for $\xi = .14$ are impacted by the resolution of the mesh; however, more detailed results are shown in Fig. 2. Numerical measurements are taken at the centerline.

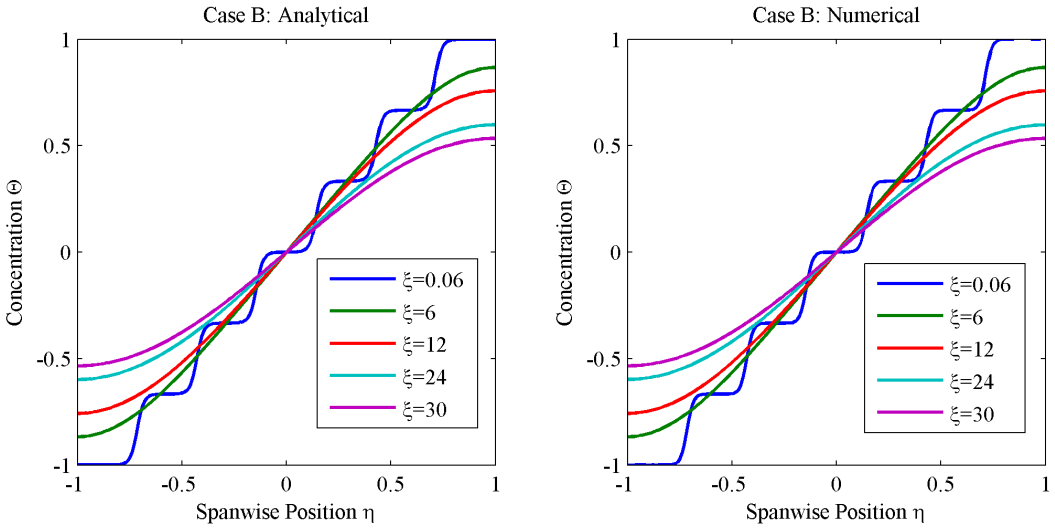

Figure 4: Concentration profiles for case B at several streamwise positions. As in case A, the analytical and numerical predictions show excellent agreement.

5 Conclusion

Overall, the analytical model appears to accurately predict concentration profiles in practically relevant cases. It could prove useful both in performing rough calculations of concentration profiles during device design, and in optimizing device geometries and flow rates. Further development of the model could center around the effects of flow attenuation near the edges of the chamber, or on determining a smallness parameter which better describes the regime in which the model is accurate. Finally, comparison with experimental data, as opposed to numerical predictions, could provide much more rigorous validation.

References

[1] F. Lin, C. M. C. Nguyen, S. J. Wang, W. Saadi, S. P. Gross, and N. L. Jeon, "Effective neutrophil chemotaxis is strongly influenced by mean il-8 concentration," *Biochemical and Biophysical Research Communications*, vol. 319, no. 2, pp. 576–581, 2004.

[2] D. Irimia, D. A. Geba, and M. Toner, "Universal microfluidic gradient generator," *Analytical Chemistry*, vol. 78, no. 10, pp. 3472–3477, 2006.